Journal of Sound and Vibration 330 (2011) 1582–1598

Contents lists available at ScienceDirect

Journal of Sound and Vibration

journal homepage: www.elsevier.com/locate/jsvi

Dynamic vibration absorbers for vibration control within a frequency band

Cheng Yang, Deyu Li, Li Cheng*

Department of Mechanical Engineering, The Hong Kong Polytechnic University, Hong Kong, China

ARTICLE INFO

Article history:
Received 24 May 2010
Received in revised form
12 October 2010
Accepted 12 October 2010
Handling Editor: J. Lam
Available online 13 November 2010

ABSTRACT

The use of dynamic vibration absorbers to control the vibration of a structure in both narrow and broadbands is discussed in this paper. As a benchmark problem, a plate incorporating multiple vibration absorbers is formulated, leading to an analytical solution when the number of absorbers yields one. Using this analytical solution, control mechanisms of the vibration absorber in different frequency bandwidths are studied; the coupling properties due to the introduction of the absorber into the host structure are analyzed; and the control performance of the absorber in different control bandwidths is examined with respect to its damping and location. It is found that the interaction between the plate and the absorber by means of the reaction force from the absorber plays a dominant role in a narrow band control, while in a relatively broadband control the dissipation by the absorber damping governs the control performance. When control bandwidth further enlarges, the optimal locations of the absorbers are not only affected by the targeted mode, but also by the other plate modes. These locations need to be determined after establishing a trade-off between the targeted mode and other modes involved in the coupling. Finally, numerical findings are assessed based on a simply-supported plate and a fair agreement between the predicted and measured results is obtained.

1. Introduction

Dynamic vibration absorbers (DVA) are widely used for the control of structural vibration and noise radiation owing to their simplicity, effectiveness, and inherent stability characteristics. The working principle of a DVA has long been demonstrated by Ormondroyd and Den Hartog [1] using a single degree of freedom (sdof) system subject to harmonic excitation. Historically, the DVA first found its utilization in the vibration control at a single frequency, predominantly at the resonance frequency of the system [2,3]. Applications of DVA have then been extended to various applications such as vibration control of machinery and structures, exemplified by a large number of works reported in literatures [4,5]. Alternatively, the absorber can be tuned to the excitation frequency [6]. In order to track the change of excitation frequency, semi-active [7] and active vibration absorbers [8] have also been explored.

A DVA is also used to suppress vibration over a frequency band, generally in the vicinity of a targeted frequency. In this circumstance, a good trade-off between the suppressed original peak and the two newly emerged coupled peaks induced by the insertion of the absorber is crucial to obtain a global vibration reduction within the frequency band of interest. For sdof systems, the well-known fixed-point method was presented [9], and the absorber was found to be most favorably tuned

* Corresponding author.
E-mail address: mmlcheng@polyu.edu.hk (L. Cheng).

0022-460X/$ - see front matter © 2010 Elsevier Ltd. All rights reserved.
doi:10.1016/j.jsv.2010.10.018

when the two coupled peaks lying inside the frequency range have equal amplitude [10]. For multiple degrees of freedom (mdof) or continuous systems, the tuning process becomes more delicate as the absorber is coupled with all structural modes of the host systems. The vibration of a cantilever beam with attached absorbers was theoretically discussed in [2,3]. Free and forced vibrations of a plate with embedded DVAs were also analytically investigated in [11–13]. It was observed that the insertion of DVAs into the host structure reconstructs the contribution of modal response [14], which in turn affects the characteristics of the system and thus appeals for a proper selection of absorber parameters, such as damping and location. This brought up the issue of optimization of DVA parameters. A substructure technique for minimizing the vibration of a continuous system over separate bands was proposed in [15], in which a DVA performance index defined in terms of the DVA damping was examined. Later, the effect of the absorber damping on the control performance was investigated using a simply-supported plate [16], but the effect of the absorber location was not discussed. An expression for optimal damping was derived in [17], and therein the absorber location was studied as well. It was found that a properly positioned DVA can provide a good global control over quite a wide frequency range. The optimal location for a cantilever beam subject to various spatial excitations was examined by Jacquot [18]. More recently, Howard et al. [19] implemented a parallel genetic algorithm to optimize the locations, stiffness, and damping of a large number of DVAs and Helmholtz resonators (HR) for a payload vehicle. Deploying a distributed computing network of 150 computers, simulations showed an overall reduction of the acoustic potential energy in a broad frequency band.

It is evident that the band control capability of DVAs aroused great interest due to its practical application value. Despite the persistent effort made in the past, however, several key issues have not been fully understood. Two aspects are on the top of the list. First, the working mechanism of DVA may differ as the frequency bandwidth changes. This will impact on the tuning of the DVA parameters to achieve the optimal band control performance. Second, both the insertion of DVAs and the enlargement of the frequency band may result in a more active coupling among structural modes, which in turn affects the optimal location of the DVAs. A good understanding of these two issues can not only help reveal the physical insight on the interaction between absorber and host system but also give guidance to the design of DVAs for practical engineering applications. This study attempts to explore these fundamental issues using a simple plate system as the benchmark system. More specifically, DVAs are used to control the resonant responses within different bandwidths. The underlying control mechanisms of DVAs are examined through investigating the absorber parameters, such as damping and locations. This has been achieved by establishing a general model consisting of a plate incorporating multiple DVAs. When the number of DVAs retreats to one, an analytical expression for the displacement of the plate is derived. With this solution, the control mechanism of a DVA is investigated. Two major effects of a DVA, reaction and dissipation, are shown to be dependent on the control bandwidth. Then the optimal absorber locations for controlling well-separated modes or closely packed modes are examined together with a method to suppress the adverse effect at those off-targeted resonances. Experiments are then conducted to validate the numerical findings.

2. Theory

A plate is chosen as benchmark structure due to its simplicity in modeling. For the completeness of the paper, the modeling procedure is briefly summarized in the following sections. The system under consideration consists of a homogeneous, orthotropic, and thin rectangular plate with M DVAs, as shown in Fig. 1. The plate is subject to a harmonic point force of $Fe^{i\omega t}$ at (x_0, y_0).

2.1. General coupled model of a plate with DVAs

The motion of the nth absorber follows the Newton's second law as

$$m_n\ddot{z}_n(t)+c_n\dot{z}_n(t)+k_nz_n(t)=c_n\dot{w}(x_n,y_n,t)+k_nw(x_n,y_n,t), \tag{1}$$

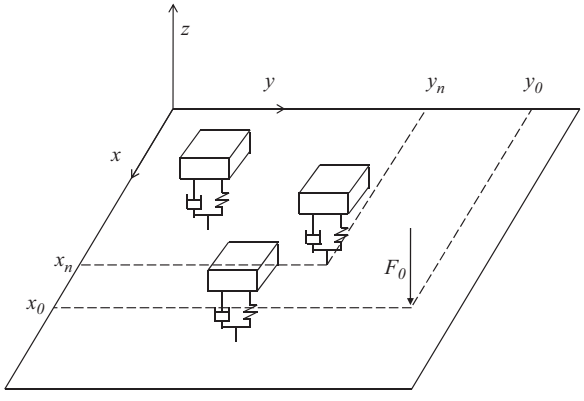

Fig. 1. A plate incorporating multiple dynamic vibration absorbers.

where $z_n(t)$, m_n, c_n, and k_n represent the displacement, mass, damping constant, and stiffness of the nth absorber, respectively; $w(x_n, y_n, t)$ is the lateral displacement of the plate at the absorber location (x_n, y_n).

Under harmonic excitation at an angular frequency ω, the equation of motion for the plate is expressed as [16]

$$D\nabla^4 w(x,y)-\omega^2\rho w(x,y)=F\delta(x-x_0)\delta(y-y_0) \quad +\sum_{n=1}^{M}(\mathrm{i}\omega c_n[Z_n-w(x_n,y_n)]+k_n[Z_n-w(x_n,y_n)])\delta(x-x_n)\delta(y-y_n), \tag{2}$$

where D is the flexural rigidity of the plate, ρ the area density, δ the Dirac delta function, and Z_n the displacement amplitude of $z_n(t)$.

Using modal expansion method, the displacement $w(x, y)$ of the plate can be expanded on the basis of mode shapes of the plate as $w(x,y)=\sum_{j=1}^{J} W_j\Phi_j(x,y)$, where W_j is the jth modal displacement, $\Phi_j(x, y)$ is the jth mode shape, and J is the maximum mode number used in computation. Making use of the orthogonality property of the mode shapes, a set of decoupled equations can be obtained from Eq. (2) as

$$\beta_j^2 W_j-\omega^2 W_j+\mathrm{i}2\omega\xi_j\beta_j W_j=F\frac{\Phi_j(x_0,y_0)}{M_j}+\omega^2\sum_{n=1}^{M}\frac{m_n}{M_j}Z_n\Phi_j(x_n,y_n) \quad (j=1,2,\ldots,J), \tag{3}$$

where β_j is the jth natural angular frequency, M_j is the jth modal mass, represented as $M_j=\rho\int_S[\Phi_j(x,y)]^2\,\mathrm{d}x\,\mathrm{d}y$, ξ_j is the jth modal damping ratio, and S is the plate area. Notice that the term $\mathrm{i}2\omega\xi_j\beta_j W_j$ on the left hand side has been introduced to represent the damping effect of the plate.

Now substituting the modal expansion expression of the plate displacement into Eq. (1), the distance amplitude Z_n of the nth DVA is obtained as

$$Z_n=T_n\sum_{h=1}^{H}W_h\Phi_h(x_n,y_n), \tag{4}$$

where T_n is a dynamic parameter defined as

$$T_n=\frac{\omega_n^2+\mathrm{i}2\xi'_n\omega\omega_n}{\omega_n^2-\omega^2+\mathrm{i}2\xi'_n\omega\omega_n},$$

where ξ'_n and ω_n are the damping ratio and the natural angular frequency of the nth DVA, respectively. Substituting Eq. (4) into Eq. (3) yields

$$\left((\beta_j^2-\omega^2+\mathrm{i}2\xi_j\omega\beta_j)-\omega^2\sum_{n=1}^{M}T_n\frac{m_n}{M_j}\Phi_j^2(x_n,y_n)\right)W_j-\omega^2\sum_{h\neq j}^{H}\sum_{n=1}^{M}T_n\frac{m_n}{M_j}\Phi_h(x_n,y_n)\Phi_j(x_n,y_n)W_h=\frac{\Phi_j(x_0,y_0)}{M_j}F \tag{5}$$

The above equation involves J modes. It should be stated that, actually, Eq. (5) is a linear system of equations in terms of the modal response W_j. W_j can be numerically solved provided the plate mode shapes are known and detailed information of the DVAs and excitation force are given. In the absence of DVA, i.e. T_n=0, the modal amplitude is solved as

$$(W_j)_{\text{without DVA}}=\frac{1}{\beta_j^2-\omega^2+\mathrm{i}2\xi_j\omega\beta_j}\frac{\Phi_j(x_0,y_0)}{M_j}F. \tag{6}$$

2.2. Analytical solution with a single DVA

Assuming only the nth DVA is installed on the plate, Eq. (5) is simplified to

$$(\beta_j^2-\omega^2+\mathrm{i}2\xi_j\omega\beta_j)W_j-\omega^2T_n\frac{m_n}{M_j}\Phi_j(x_n,y_n)\sum_{h=1}^{H}W_h\Phi_h(x_n,y_n)=\frac{\Phi_j(x_0,y_0)}{M_j}F. \tag{7}$$

Dividing $m_n/M_j\Phi_j(x_n,y_n)$ over all the terms in Eq. (7) gives

$$\frac{(\beta_j^2-\omega^2+\mathrm{i}2\xi_j\omega\beta_j)W_j}{(m_n/M_j)\Phi_j(x_n,y_n)}-\omega^2T_n\sum_{h=1}^{H}W_h\Phi_h(x_n,y_n)=\frac{\Phi_j(x_0,y_0)}{\Phi_j(x_n,y_n)}\frac{F}{m_n}. \tag{8}$$

Notice that the second term on the left hand side of Eq. (8) is independent of index j. Changing the running index with integer g gives another equation as

$$\frac{(\beta_g^2-\omega^2+\mathrm{i}2\xi_g\omega\beta_g)W_g}{\Phi_g(x_n,y_n)(m_n/M_g)}-\omega^2T_n\sum_{h=1}^{H}W_h\Phi_h(x_n,y_n)=\frac{\Phi_g(x_0,y_0)}{\Phi_g(x_n,y_n)}\frac{F}{m_n}. \tag{9}$$

Subtracting Eqs. (8) and (9) yields

$$\frac{(\beta_j^2-\omega^2+\mathrm{i}2\xi_j\omega\beta_j)W_j}{\Phi_j(x_n,y_n)(m_n/M_j)}-\frac{(\beta_g^2-\omega^2+\mathrm{i}2\xi_g\omega\beta_g)W_g}{\Phi_g(x_n,y_n)(m_n/M_g)}=\left(\frac{\Phi_j(x_0,y_0)}{\Phi_j(x_n,y_n)}-\frac{\Phi_g(x_0,y_0)}{\Phi_g(x_n,y_n)}\right)\frac{F}{m_n}. \tag{10}$$

Eq. (10) establishes a direct relationship between any two arbitrary plate modes, g and j. In this case, the modal response W_g can be expressed in terms of W_j, and substituting the new W_g expression into the independent term in Eq. (8) gives

$$\frac{\beta_j^2-\omega^2+\mathrm{i}2\xi_j\omega\beta_j}{\Phi_j(x_n,y_n)(m_n/M_j)}\left(1-m_n\omega^2T_n\sum_{h=1}^{H}\frac{\Phi_h^2(x_n,y_n)}{(\beta_h^2-\omega^2+\mathrm{i}2\xi_h\omega\beta_h)M_h}\right)W_j$$
$$=\left(1-m_n\omega^2T_n\sum_{h=1}^{H}\frac{\Phi_h^2(x_n,y_n)}{(\beta_h^2-\omega^2+\mathrm{i}2\xi_h\omega\beta_h)M_h}\right)\frac{\Phi_j(x_0,y_0)}{\Phi_j(x_n,y_n)}\frac{F}{m_n}+\omega^2T_n\sum_{h=1}^{H}\frac{\Phi_h(x_0,y_0)\Phi_h(x_n,y_n)F}{M_h(\beta_h^2-\omega^2+\mathrm{i}2\xi_h\omega\beta_h)}. \tag{11}$$

Therefore, an analytical solution of W_j is obtained from Eq. (11) as

$$W_j=\underbrace{\frac{1}{\beta_j^2-\omega^2+\mathrm{i}2\xi_j\omega\beta_j}\frac{\Phi_j(x_0,y_0)}{M_j}F}_{\text{Contribution from the primary force}}+\underbrace{\frac{1}{\beta_j^2-\omega^2+\mathrm{i}2\xi_j\omega\beta_j}\frac{\Phi_j(x_n,y_n)}{M_j}F_{\text{second}}}_{\text{Contribution from the DVA}}, \tag{12}$$

where

$$F_{\text{second}}=\frac{m_n\omega^2T_n\sum_{h=1}^{H}\frac{\Phi_h(x_0,y_0)\Phi_h(x_n,y_n)F}{M_h(\beta_h^2-\omega^2+\mathrm{i}2\xi_h\omega\beta_h)}}{1-m_n\omega^2T_n\sum_{h=1}^{H}\frac{\Phi_h^2(x_n,y_n)}{M_h(\beta_h^2-\omega^2+\mathrm{i}2\xi_h\omega\beta_h)}}. \tag{13}$$

The above analytical expression provides insightful information about the jth modal amplitude when a single DVA is attached on the plate. Eq. (12) clearly shows that the modal amplitude is composed of two parts: one is the effect induced by the primary exciting force (first term) and the second part comes from the reaction force by the DVA (second term). It is also seen in Eq. (13) that the absorber is coupled with all plate modes. This fully coupled term F_{second} represents the reaction force of the DVA on the plate. It is noted that Eq. (7) and its analytical solution Eq. (12) can be applied to the situation in which there are M identical DVAs attached at the same place (x_n, y_n), but each DVA has only $1/M$ mass of m_n. It indicates that M identical DVAs installing in the same place are equivalent to one DVA having the same resonance frequency and damping but a mass of overall.

Assuming only one targeted mode, i.e. the jth mode, dominates the response, Eq. (12) can be expressed in a dimensionless form as

$$Q=\frac{W_j}{(W_j)_{\text{without DVA}}}=\frac{1}{1-\frac{\mu_{nj}\omega^2T_n\Phi_j^2(x_n,y_n)}{\beta_j^2-\omega^2+\mathrm{i}2\xi_j\omega\beta_j}}, \tag{14}$$

where μ_{nj} is the ratio of the nth absorber mass to the jth modal mass of plate. It can be seen from Eq. (14) that Q depends on its dynamic parameter T_n and the absorber mass ratio μ_{nj}. As an extreme case, if the attachment is made at the node of the jth mode, i.e. $\Phi_h(x_n, y_n)=0$, the reacting force becomes 'contributiveless' to the modal displacement at this mode.

2.3. Qualification of the control performance

To assess the performance of the DVA, an 'energy reduction index' is defined as

$$E_r=10\log_{10}\frac{E_b^0}{E_b^1}, \tag{15}$$

where E_b^1 and E_b^0 are averaged kinetic energy of the plate within a chosen bandwidth $[\omega_1, \omega_2]$ with and without DVAs, respectively. The following expression can be used to calculate the averaged kinetic energy E_b:

$$E_b=\int_{\omega_1}^{\omega_2}\frac{1}{2}M\langle V^2\rangle\,\mathrm{d}\omega, \tag{16}$$

where M is the mass of the plate and $\langle V^2\rangle$ is the averaged quadratic velocity of the plate, which is computed by

$$\langle V^2\rangle=\frac{\omega^2}{S}\int_S w(x,y)w^*(x,y)\,\mathrm{d}x\,\mathrm{d}y, \tag{17}$$

where the asterisk denotes complex conjugate.

The energy dissipated by the DVA damping in one period T can be calculated by

$$E_d=\frac{1}{2}\int_0^T c_n\omega^2\left|z_n(t)-w(x_n,y_n,t)\right|^2\mathrm{d}t, \tag{18}$$

where $[z_n(t)-w(x_n, y_n, t)]$ is the relative displacement between the plate and the DVA at the attaching point.

For the harmonic motion, Eq. (18) is simplified as

$$E_d=\tfrac{1}{4}Tc_n\omega^2\left|Z_n-w(x_n,y_n)\right|^2. \tag{19}$$

The work done by the reacting force within the bandwidth is calculated by

$$E_f = \int_{\omega_1}^{\omega_2} \frac{1}{2} k_n |Z_n - w(x_n, y_n)|^2 \, d\omega. \tag{20}$$

3. Control mechanism and coupling analysis in different frequency bandwidths

In this section a simply-supported aluminum plate as shown in Fig. 2(a), having a dimension of $0.41 \times 0.45 \times 0.003$ m^3 is used. The coordinate system used in the study is also indicated in the figure. A primary excitation point force is exerted at (0.28 m, 0.38 m). A total of 20×20 modes are used in the simulation, which was found sufficient to ensure the accuracy of the results in the frequency range of interest up to 400 Hz. The frequency response function (FRF) of the plate observed at (0.17 m, 0.20 m) is plotted in Fig. 2(b). It can be seen that the first mode (1, 1) at 85 Hz is well-separated from all other modes, while the second mode (1, 2) at 200 Hz has a close neighboring mode (2, 1) at 224 Hz. Compared with the well-separated mode, the second and the third modes close each other, they are denoted as a closely packed mode pair. Both of these two kinds of modes (well-separated mode and closely packed mode) are examined in the following study.

As mentioned previously, the modal displacement of the plate can be calculated by Eq. (12) under the use of a single DVA in vibration control. Obviously for the plate integrated with an absorber, F_{second} relates to the absorber location (x_n, y_n), the lumped mass, and damping if traced back to Eq. (13). In practical engineering field, the lumped mass used by the DVA is expected to be small since it is not desirable to influence the characteristic of the plate due to the additional mass. In this paper the absorber damping and location are to be discussed but the effect of the absorber mass to the control performance is out of concern of the current paper.

3.1. Control mechanism of DVA for different bandwidths

The FRF of the plate centered at 85 Hz with and without a DVA is calculated at an arbitrary point of (0.17 m, 0.20 m). The absorber is tuned at the resonance 85 Hz and the mass is set as 1% of the plate, i.e. 0.015 kg. DVAs with three typical damping

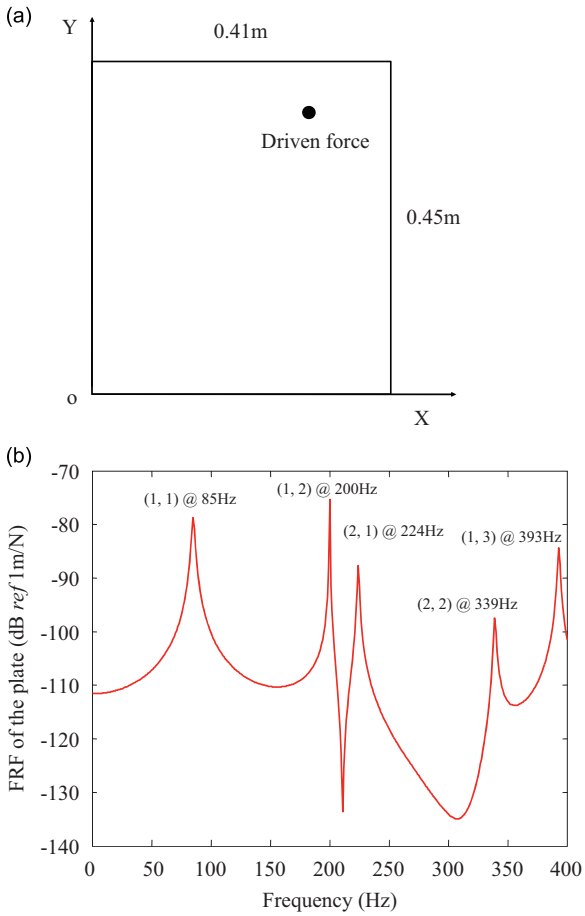

Fig. 2. (a) Coordinate system of the plate and (b) predicted FRF of the plate at (0.17 m, 0.20 m) without DVA.

values (ξ=0.012, 0.041, and 0.088) are compared to show the effect of the damping on the control performance. Notice that the case corresponding to ξ=0.041 was obtained as the result of optimization to achieve the best global control performance within a frequency band of 20 Hz, which will be detailed later in this section. It can be seen from Fig. 3 that for the relatively low damping, i.e. ξ=0.012, although the reduction is significant at the central frequency of 85 Hz, a pair of new peaks appear. Judging from the peak values within the bandwidth, only a reduction of 4.2 dB is achieved. Increasing the damping ratio to the optimal one, i.e. ξ=0.041, these two new peaks are smoothed down, leading to a reduction of 8.7 dB. By further increasing the damping ratio to ξ=0.088, the two coupled peaks disappear to form a single peak, resulting in a vibration reduction of 7.8 dB. Obviously, the lightly damped absorber can perfectly suppress the vibration only at the resonance frequency. The fierce vibration at this frequency is pinned by the reaction force from the absorber. If a wide frequency band is considered, however, the control mechanism would be different. In this case, a proper balance between the absorber damping and the selected bandwidth is needed.

When attaching a DVA on a host structure, the DVA vibrates due to the excitation from the host structure. One part of the input energy to the DVA is dissipated through its damping, and the remaining energy returns back to the host system by means of the reacting force to form an interaction between the DVA and the structure. Therefore, the dual process of dissipation and interaction co-exists and form the control mechanism of the DVA. This issue is first investigated by choosing a relatively wide bandwidth of 20 Hz centered at 85 Hz. The energy reduction of the plate, the dissipation energy by the DVA, and the work done by the reacting force are calculated using Eqs. (15), (19) and (20) for different DVA damping ratios. Results are shown in Fig. 4(a–c). Fig. 4(a) shows that, at low damping, the increase of damping benefits the energy reduction E_r of the host structure, and a maximum reduction of 3.8 dB is reached when the damping ration is ξ=0.041. After that, the continuous increase of damping weakens the energy reduction. Albeit slight differences in the peak position, a similar trend is observed in the bandwidth energy dissipation E_d of the DVA, as illustrated in Fig. 4(b). The tendency match between E_d and E_r suggests that in a relatively large bandwidth, e.g. 20 Hz, the energy reduction of the host system is dominated by the dissipation of DVA, and thus, the dissipation capability of the absorber determines the vibration reduction of the plate. But a threshold exists beyond which no further energy reduction can be achieved. It is worth noting that the optimal damping for E_r (ξ=0.041) and E_d (ξ=0.039) are slightly different. This means although the control performance is governed by the dissipation mechanism of the DVA in the case of a large bandwidth, the optimal damping for maximum vibration reduction cannot be simplified as the maximization of the energy dissipation by the DVA. Fig. 4(c) also suggests a strong coupling between the absorber and plate at low damping, as evidenced by the efficient energy feedback to the plate. Excessive damping, however, reduces the motion of the absorber and therefore influences the energy transmission between the DVA and the plate, which consequently constrains the energy dissipation as well.

It is expected that the aforementioned control mechanism only applies when the frequency band of interest is relatively large to cover both the original resonance peak and the newly coupled peaks due to the insertion of the resonator. This issue is investigated hereafter. The damping ratio of DVA is determined in two different ways: (1) the damping corresponding to the

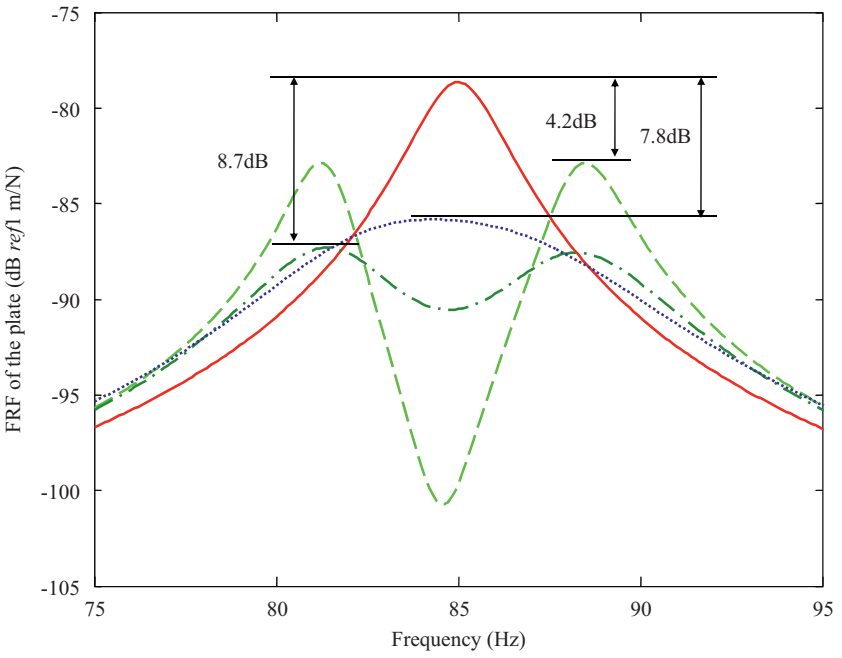

Fig. 3. Effect of the absorber damping on the FRF of the plate observed at (0.17 m, 0.20 m). ——, without DVA; — —, ξ=0.012; — ● —, ξ=0.041; ●●●●, ξ=0.088.

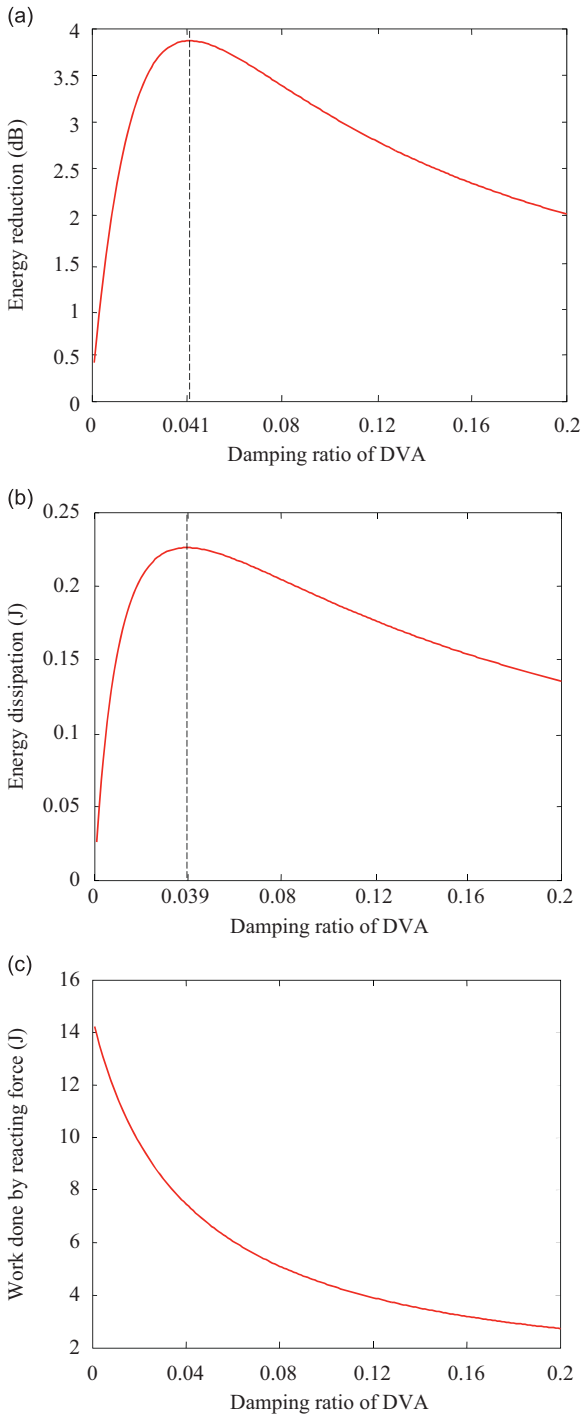

Fig. 4. Dependence of energy terms on damping ratios of the absorber in 20 Hz bandwidth: (a) energy reduction of plate, (b) energy dissipation by DVA, and (c) work done by reacting force.

maximum energy reduction of the plate is defined as the optimal damping, indicated by ξ_{red} and (2) the damping corresponding to the maximum energy dissipation of the absorber is referred to as the maximum dissipation damping, denoted by ξ_{dis}. A bandwidth varying from 0.2 to 20 Hz is chosen as the observing range which covers from narrow band to a relative wide band. The variations of ξ_{red} and ξ_{dis} against the frequency bandwidth are illustrated in Fig. 5. It is observed that when the frequency bandwidth is very small, the damping ratios determined by the above two methods has a significant

difference. As the bandwidth increase, the two damping ratios get closer. Finally, the two damping ratios are almost the same (0.04) when the bandwidth is larger than 10 Hz.

This phenomenon can better be characterized based on half-power bandwidths, (f_1-f_2) and (f_3-f_4), corresponding to the two newly emerged peaks due to the insertion of the DVA. The whole frequency bandwidth range shown in Fig. 5 can then be divided into three different zones. Zone I corresponds to a narrow bandwidth (NB), in which the control bandwidth is so narrow ($\leq f_3-f_2$) that the control region basically focuses on the resonance peak and excludes the newly emerged coupling peaks. Zone II denotes moderate bandwidth (MB), i.e. the two coupling peaks are contained within the control band, but the bandwidth is still smaller than or equal to the frequency bandwidth of (f_1-f_4). Zone III corresponds to a relatively wide bandwidth (WB) containing the two newly created peaks ($\geq f_1-f_4$) to cover the entire range where the DVA's performance remains. In zone I, the optimal damping ξ_{red} is much lower than the maximum dissipation damping ξ_{dis}. This suggests that, for the narrow-band control, the optimal DVA damping is not the one that maximizes the energy dissipation of the plate. Instead, an effective interaction between the plate and the DVA is the key element. Therefore, the control mechanism of the DVA in a narrow band control is dominated by the reacting force, i.e., by the interaction between the plate and the DVA. In zone II, as the bandwidth gradually increases, ξ_{dis} decreases drastically and approaches to the gradually increasing ξ_{red}. This suggests a growing importance of energy dissipation from the absorber. In zone III, ξ_{red} and ξ_{dis} almost coincide by undergoing only very smooth variation, which indicates that the energy dissipation has taken over as the dominating effect in the vibration reduction.

3.2. Coupling analysis in terms of bandwidths and DVA locations

As can be seen from the second term on the left hand side of Eq. (5), all structural modes are coupled with the DVA. The coupling strength obviously depends on various system parameters, among which the bandwidth of interest and the location of the DVA are considered here. To qualify the coupling effect, a bandwidth energy variation parameter EV is defined as

$$\mathrm{EV}=10\log_{10}\left(\int_{\omega_1}^{\omega_2}\frac{E_b^0}{E_b^j}\,\mathrm{d}\omega\right) \tag{21}$$

where E_b^0 is the bandwidth averaged kinetic energies of the plate when a converged solution is obtained using 400 modes, and E_b^j is the bandwidth averaged kinetic energies of the plate when the first j modes are considered in computation. In fact, EV reflects how close the bandwidth energy of the plate can be approached by using a limited number of modes. For a 20 Hz bandwidth centered at 200 Hz, the EVs before and after installing the DVA are shown in Fig. 6. It can be seen that, in the absence of absorber, EV converges very rapidly since only a few modes contribute significantly to the response. After installing the absorber, however, more modes come into play. This suggests that the presence of absorber excites more

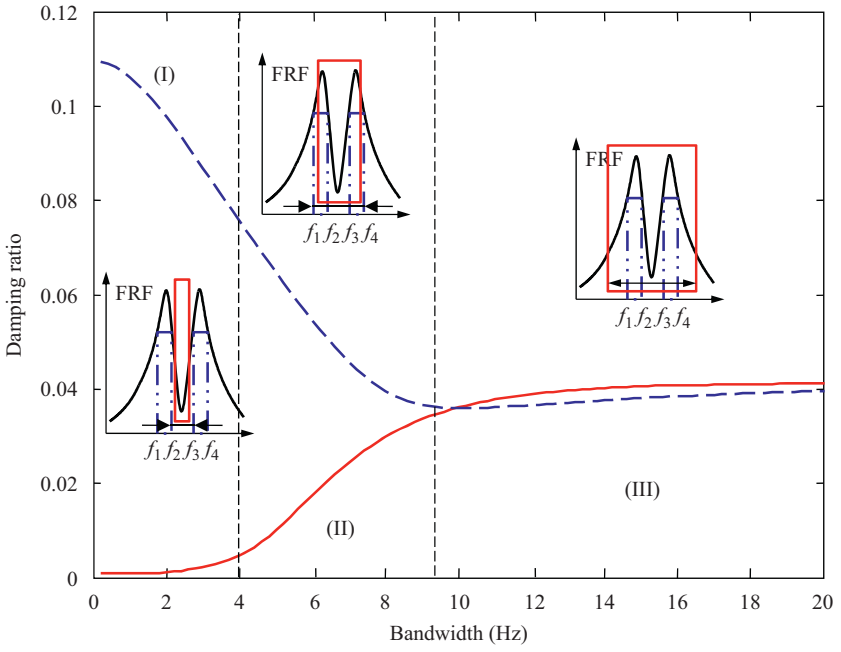

Fig. 5. Optimal damping ratio vs. bandwidth: ——, optimal damping ratio ξ_{red} from maximum energy reduction of plate; — —, damping ratio ξ_{dis} from maximum energy dissipation of DVA.

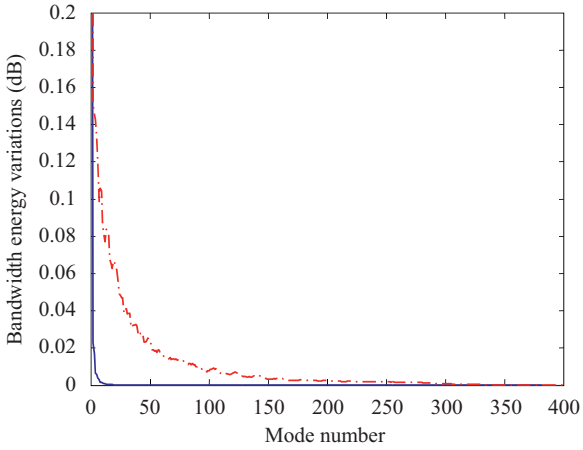

Fig. 6. 20 Hz bandwidth energy variations vs. number of plate modes before and after installing DVA. ——, without absorber; — • —, with absorber.

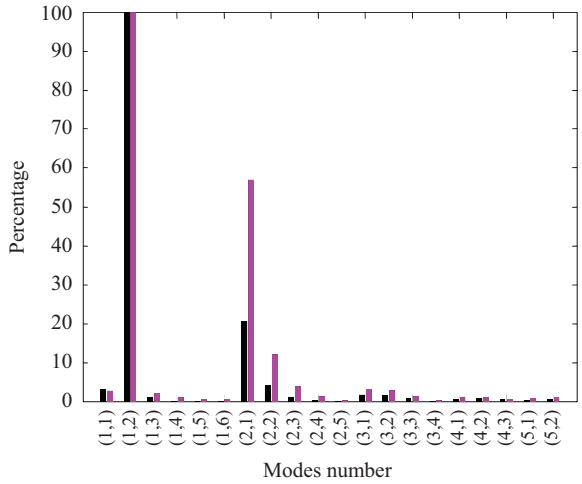

Fig. 7. Contribution percentage of each mode against the maximum mode. Dark bars, without DVA; light bars, with DVA.

structural modes, and therefore enhances the modal coupling between them. Participation of each individual mode can be better illustrated by decomposing the response of the plate into each mode. To that end, the normalized modal response of the first 20 modes is shown in Fig. 7. It is obvious that the presence of DVA activates more plate modes such (2, 1), (2, 2) and (2, 3). This increased modal coupling due to the band consideration also implies that the parameter tuning of the DVA as well as its installation requires a model, which considers the multi-modal coupling feature of the system.

Eq. (5) also shows that the absorber location is another decisive parameter affecting the structural coupling. One indication is the separation of the new coupled peaks due to the insertion of the DVA. From Eq. (14), the newly emerged resonance frequencies due to the insertion of the DVA can be determined by setting the denominator to zero, in a way similar to [17]. This results in a frequency separation between the two resonances

$$\Delta\omega_j = \beta_j |\Phi_j(x_n, y_n)| \sqrt{\mu_{nj}} \tag{22}$$

Eq. (22) shows that the separation of the resonant frequencies is proportional to the resonant frequency β_j of the targeted mode, the absorber location $\Phi_j(x_n, y_n)$, and the absorber mass ratio μ_{nj}. A change in absorber location modifies the separation, so the coupling peaks can either be excluded or included in investigated band, within which vibration reduction is expected.

3.3. Optimal DVA locations

When the mode under control is well separated from others, weak modal coupling takes place. The conventional way of locating the DVA in the anti-node region applies as evidenced by Fig. 8, in which the well-separated mode (1, 1) at 85 Hz is

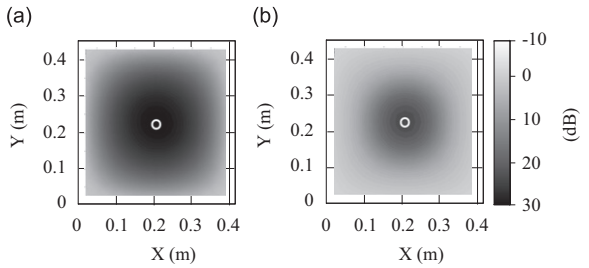

Fig. 8. Map of bandwidth energy reduction E_r for the well-separated mode. Pixels correspond to spatial points of the plate, and the field value at a pixel stands for the energy reduction calibrated by different grey-scales. The darkest area, marked by ○ corresponds to the optimal location for installing the absorber: (a) 2 Hz bandwidth and (b) 10 Hz bandwidth.

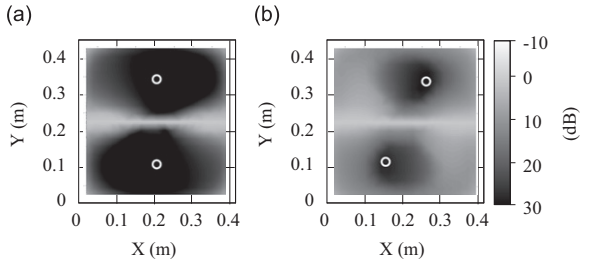

Fig. 9. Map of bandwidth energy reduction E_r for the closely packed mode. Pixels correspond to spatial points of the plate, and the field value of a pixel stands for the energy reduction calibrated by different grey-scales. The darkest area, marked by ○ corresponds to the optimal location for installing the absorber: (a) 2 Hz bandwidth and (b) 20 Hz bandwidth.

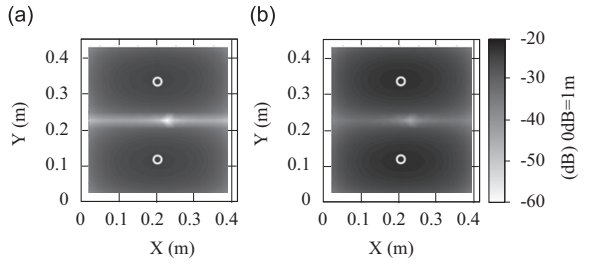

Fig. 10. Bandwidth vibration energy distribution of the plate without absorber: (a) 2 Hz bandwidth and (b) 20 Hz bandwidth. ○, maximum vibration.

investigated. In the figure, pixels correspond to spatial points of the plate. The field value of a pixel stands for the energy reduction calibrated by different grey-scales. The darkest area, marked by "○" corresponds to the optimal location for installing the absorber. Fig. 8 shows the energy reduction E_r within 2 and 10 Hz bandwidth when the DVA location varies in the plate. It can be seen that for a narrow band of 2 Hz, the preferable locations (dark region) where the absorber produces larger energy reduction (25 dB or above) occupy a large area around the center of the plate. While for 10 Hz bandwidth, the better control area (dark region) is smaller and the maximum achievable reduction is only 18 dB, 7 dB less than the result in a narrow band case. A larger variation in the magnitude of E_r is found in narrow band control, indicating that the control performance of the DVA is more sensitive to its location in the case of narrow band control.

Optimal locations of DVA for the control of closed-packed modes are then investigated. Mode (1, 2) and its neighboring mode (2, 1) are taken as an example. The control results under different bandwidths vs. the DVA location are shown in Fig. 9(a) and (b). The bandwidth vibration energy of the plate [Eq. (16)] without DVA is also given in Fig. 10 for comparisons.

It can be seen from Fig. 9 that, whilst the absorber performs well in a large region (dark region) for 2 Hz bandwidth, the optimal region for 20 Hz bandwidth is significantly reduced. Most importantly, for the narrow band, the optimal locations close to the nodal line of mode (1, 2), corresponding to the maximum vibration area as shown in Fig. 10(a). For the wide bandwidth, however, the optimal locations (0.14 m, 0.11 m) and (0.27 m, 0.34 m) are away from the maximum vibration locations, though the vibration within this band is still dominated by the mode (1, 2), as illustrated in Fig. 10(b). This shows that, with the consideration of a larger bandwidth, the DVA cannot simply be placed at the maximum vibration region. An optimization should be conducted based on a model, in which the multi-modal coupling feature of the system is considered, like the one proposed in this paper.

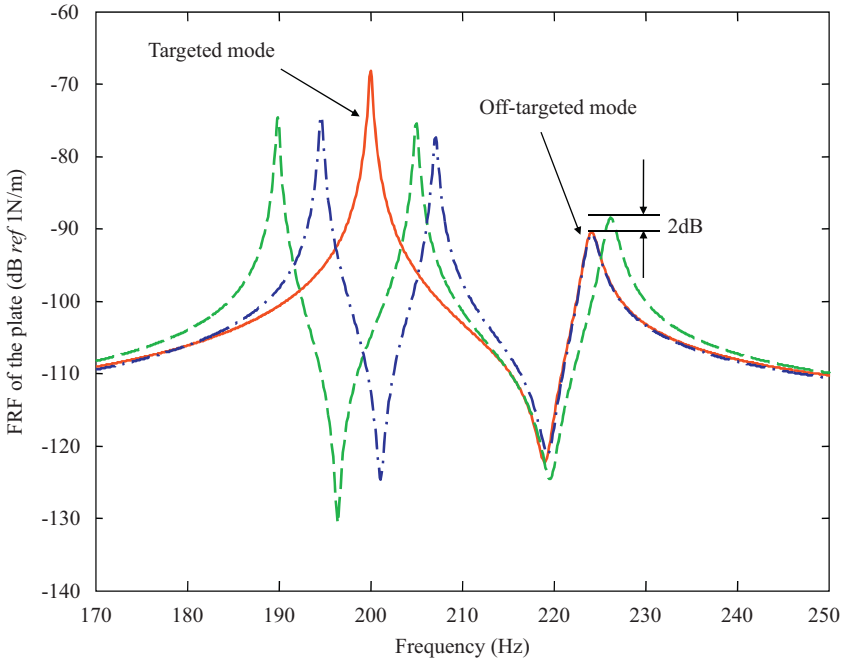

Fig. 11. Worsened effect at off-targeted mode: ——, without absorber; — —, with absorber creating an adverse effect at mode (2, 1); — • —, with absorber location optimized using Eq. (25).

3.4. *Effect of DVA on response at off-targeted modes*

When the absorber is installed on the plate, it suppresses the resonance to which it is tuned. Adverse effects may however exist at some off-targeted modes. One typical result is shown in Fig. 11, in which case when controlling the mode (1, 2), a 2 dB increase is observed at the off-targeted mode (2, 1). This is due to the dynamical coupling between the absorber and the off-targeted mode. In an extreme case, by placing the absorber on the anti-node of a certain off-targeted mode M, the zero value of mode shape $\Phi_M(x,y)$ disables the coupling between the absorber and mode M. But in a more likely case where $\Phi_M(x,y)\neq 0$, assuming only the M mode dominates in the response at its resonant frequency ω_M, the adverse effect can be suppressed as $|W_0(\omega_M)| < |W_1(\omega_M)|$, where W_0 and W_1 denote the modal displacement before and after the installation of absorber. From Eq. (6) and (12), it gives

$$W_1(\omega_M)-W_0(\omega_M)=\frac{\frac{\Phi_j(x_n,y_n)}{M_j}}{\beta_j^2-\omega_M^2+\mathrm{i}2\xi_j\omega_M\beta_j}\frac{m_n\omega_M^2T_n\sum_{h=1}^{H}\frac{\Phi_h(x_0,y_0)\Phi_h(x_n,y_n)F}{M_h(\beta_h^2-\omega_M^2+\mathrm{i}2\xi_h\omega_M\beta_h)}}{1-m_n\omega_M^2T_n\sum_{h=1}^{H}\frac{\Phi_h^2(x_n,y_n)}{M_h(\beta_h^2-\omega_M^2+\mathrm{i}2\xi_h\omega_M\beta_h)}}. \tag{23}$$

By imposing $|W_1(\omega_n)-W_0(\omega_n)|=0$, an expression with respect to the absorber location is obtained as

$$\left|\sum_{h=1}^{H}\frac{\Phi_h(x_0,y_0)\Phi_h(x_n,y_n)F}{M_h(\beta_h^2-\omega_M^2+\mathrm{i}2\xi_h\omega_M\beta_h)}\right|=0. \tag{24}$$

Apparently, the variation of absorber location affects the response at the off-targeted mode and the adverse effect can be eliminated if placing the absorber properly. Expression (24) provides an additional criterion that can be used for determining the optimal locations of the DVA coping with multi-range consideration. Upon applying this criterion, Fig. 11 shows that the adverse effect can be eliminated without sacrificing the control performance at the targeted mode.

4. Experimental validations

Measurements are conducted to validate the results presented above. In Fig. 12(a), a simply-supported aluminum plate, having the same dimension as the one used in simulation, is fabricated and installed on an isolation table [20]. In order to achieve a simply-supported boundary condition, a strip of V groove was carved at each side of the plate along the edge. The rims of the plate (outside the V grooves) were clamped by steel-made frames with a thickness of 40 mm (front frame) and 80 mm (back frame), respectively [see Fig. 12(a) for details]. The frame was initially supported by a pair of oblique bars installed at the back of the frame. However, measurements showed that this turned out to be unnecessary, and only the frame itself could provide a large enough stiffness in the transverse direction of the plate. A single point primary force is applied at (0.28 m, 0.38 m) using a Brüel & Kjær Type 4809 shaker. Vibrations are measured using a PSV-400 Scanning Laser-vibrometer.

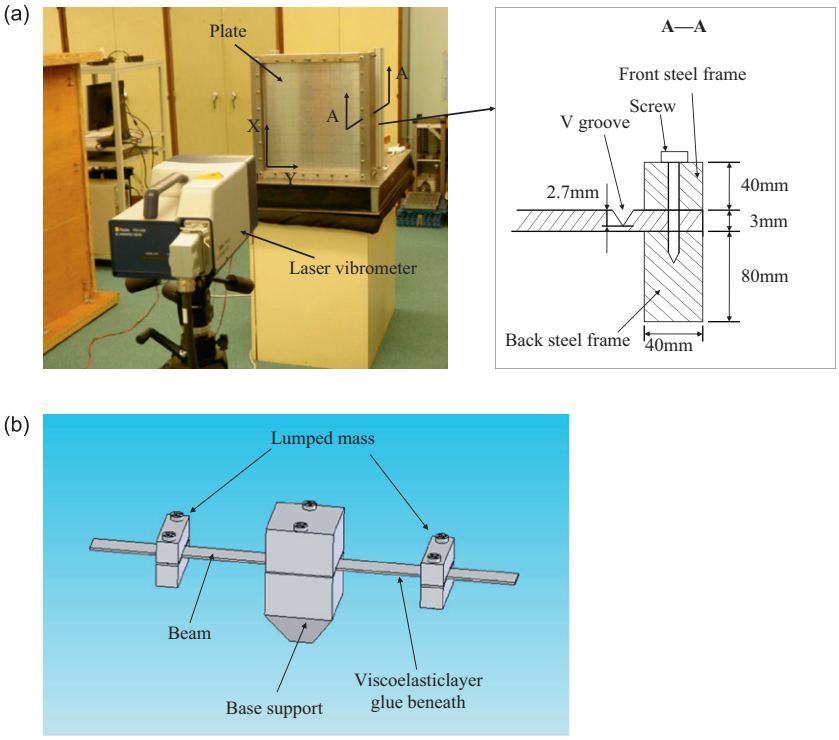

Fig. 12. Experimental set-up: (a) test bed and (b) beam-mass type DVA.

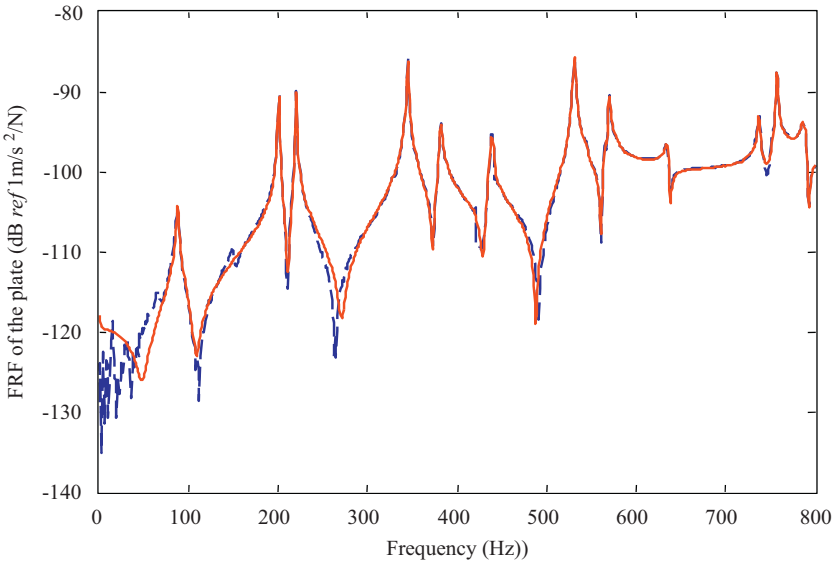

Fig. 13. FRF curves of the plate observed at (0.123 m, 0.113 m) without DVAs. ——, predicted result; — —, measured result.

The measured and computed FRF curves of the plate at location (0.123 m, 0.113 m) are compared in Fig. 13. In the computation, the experimentally identified damping ratios are used (see Table 1). The good match between the measured and predicted curves in the frequency range of interest shows that the simply-supported boundary conditions of the plate used in the experiment is well satisfied. It should be noted that an alternative and probably more reasonable way of representing the structural damping of a system in the theoretical development is to use the hysteretic damping instead of viscous damping [21]. In our case, modal damping ratio was obtained by measurement. The agreement between the model and measurement

Table 1
Computed natural frequencies and measured damping ratios.

Index	Mode no.	Natural freq. (Hz)	Damping ratio
1	(1, 1)	85	0.0147
2	(1, 2)	200	0.0016
3	(2, 1)	224	0.0011
4	(2, 2)	339	0.0020
5	(1, 3)	393	0.0038
6	(3, 1)	456	0.0035
7	(2, 3)	532	0.0032
8	(3, 2)	571	0.0019
9	(1, 4)	662	0.0015
10	(3, 3)	764	0.0024
11	(4, 1)	780	0.0029
12	(2, 4)	801	0.0025

shown in Fig. 13 demonstrate that the viscous damping model can well satisfy the prediction accuracy required in this analysis.

4.1. Optimal damping

In order to reduce the moment effect on the interactions between the plate and the DVA, the DVA is designed and fabricated using two identical back to back beam-mass elements, symmetrically arranged with respect to the central axis, as shown in Fig. 12(b). As mentioned in Section 2.2, the two identical absorbers are equivalent to one absorber with the same resonance frequency and damping but doubled lumped mass. The dynamics of each beam-mass system can be approximated as a single degree of freedom system assuming that only the first mode of the beam dominates [22]. Therefore, the beam serves as a spring and a distributed mass. By adjusting the location of the lumped mass on the beam, the effective stiffness of the spring can be changed, and in turn, the working resonance frequency of the DVA can be tuned. Initial design of the absorber is based on the estimated natural frequency of the system using formulas in [23]. The final configuration is then finely tuned experimentally. The damping ratio of the absorbers was tuned by applying a damping layer coated on the surface of the beam. Commercially available damping liquid, SWEDAC DG-U 6, is applied to the surface of the beam. By controlling the thicknesses of the coating layer, different damping ratio of the DVA can be obtained. It should be noted that the support part of the DVA increases the total mass of the absorber. As demonstrated by Eq. (22), the increase of the absorber mass will widen the separation of the coupled resonances. For the current configuration, the mass ratio of the base support to the modal mass of the plate is only 0.6%, which results in 1.2 Hz increase in the frequency separation for the first mode. Thus the influence of the support part is small as it is relatively light compared with the plate.

The vibration control at the first resonance of 85 Hz using the DVA is carried out. The FRF of the plate with an absorber is measured at (0.17 m, 0.20 m) and shown in Fig. 14. Similar to the simulation implemented in Fig. 3, the beam-mass absorbers are designed to have three typical damping ratios as those used in simulations. Due to the practical difficulty in getting exactly the desired optimal damping value ($\xi_{\mathrm{red}}=0.041$), the best achieved damping used in the experiment is $\xi=0.039$, which is near the optimal result. With this damping, a 6.8 dB reduction is achieved, which is 1 dB smaller than the predicted result. For the small and large damping, the two sharp peaks and the single peak occur, respectively, consistent with numerical predictions. In general, the control performance of each absorber agrees with the numerical results to an acceptable extent and the optimal damping obtained is capable to provide the highest reduction.

4.2. Optimal location of DVA

The optimal location of absorber for vibration control in a frequency band is also experimentally validated. The closely packed mode (1, 2) at 200 Hz is chosen. In a bandwidth of 20 Hz centered at 200 Hz, the maximum displacement amplitude at each node of a 20×20 grid over the plate is measured using PSV-400 without DVA. It is seen from Fig. 15 that the vibration finds its maximum at the regions around the anti-node and a minimum vibration region distributes in the midline of the plate, which indicates that the vibration within this band is dominated by the targeted mode (1, 2). Then, the DVA is, respectively, placed at the location (0.205 m, 0.3375 m), which is the anti-node of the targeted mode, and the location (0.27 m, 0.34 m), which is the optimal location obtained in the simulation. The FRF of the plate (displacement) measured at the location (0.265 m, 0.162 m) is shown in Fig. 16. It is observed that after placing the DVA on the plate, the vibration at the targeted resonance 200 Hz is well suppressed. Also, it is found that the absorber placed at optimal location results in a reduction of 7.9 dB, while only a 4.6 dB reduction is achieved if the absorber is placed at the anti-node. This is also consistent with numerical results.

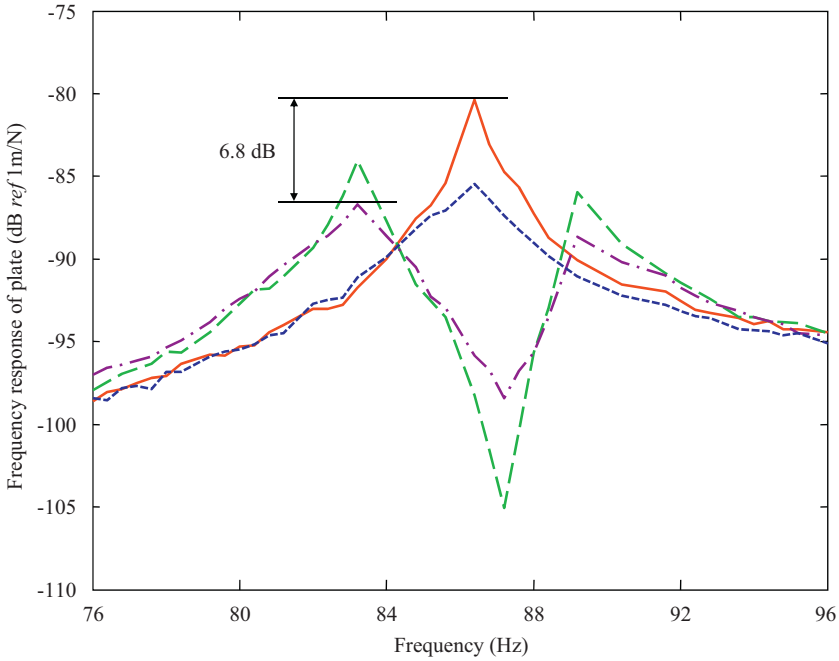

Fig. 14. Measured FRF curves of the plate observed at (0.17 m, 0.20 m). ——, without DVA; — —, ξ=0.012; — ● —, ξ=0.088; ●●●●, ξ=0.039.

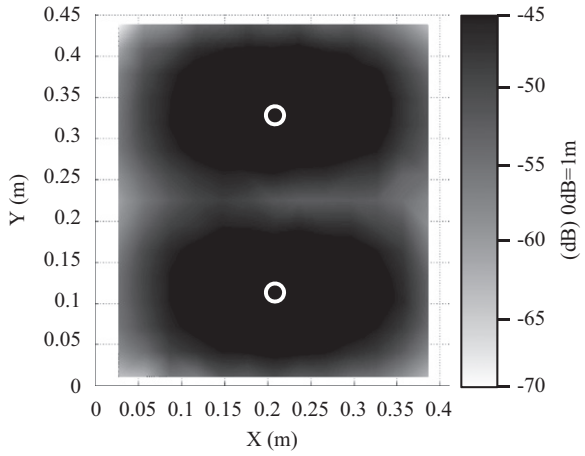

Fig. 15. Measured 20 Hz bandwidth vibration of the plate without DVA. ○, maximum vibration.

4.3. *Broadband control by using multiple DVAs*

As a final example, the capability of using multiple DVAs to achieve a broadband vibration reduction is demonstrated. When the number of DVA increases, however, a systematic optimization becomes a necessity due to the complex coupling among DVAs and the host plate. That is, a model, such as the one presented in this work, becomes indispensable. To achieve the optimal control performance of the DVAs, genetic algorithm (GA) is used in conjunction with the present model. The GA approach allows determining the optimal location of each DVA. The control object is to find the maximum energy reduction E_r in the 20 Hz bandwidth centered at each targeted resonance frequency. The implementation procedures of control using the DVAs are described as follows: (1) A DVA is first designed using the resonance frequency of the target mode. A genetic algorithm (GA) used in [24] is applied to find the optimal location for this DVA. (2) The installation of the first DVA splits the target peak into two new peaks. These two new coupled resonances are then selected as the resonance frequencies of the other two DVAs. (3) The above procedure can be repeated until the resonance frequencies of all the DVAs are fixed. After

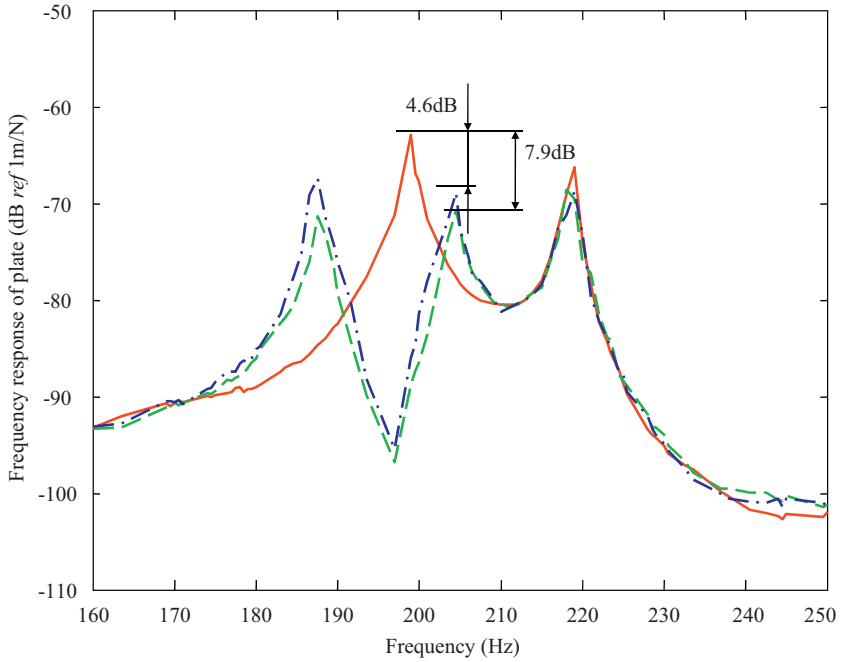

Fig. 16. FRF of the plate observed at location (0.265 m, 0.162 m). ——, without DVA; — —, DVA placed at anti-node; — • —, DVA placed at the optimum location.

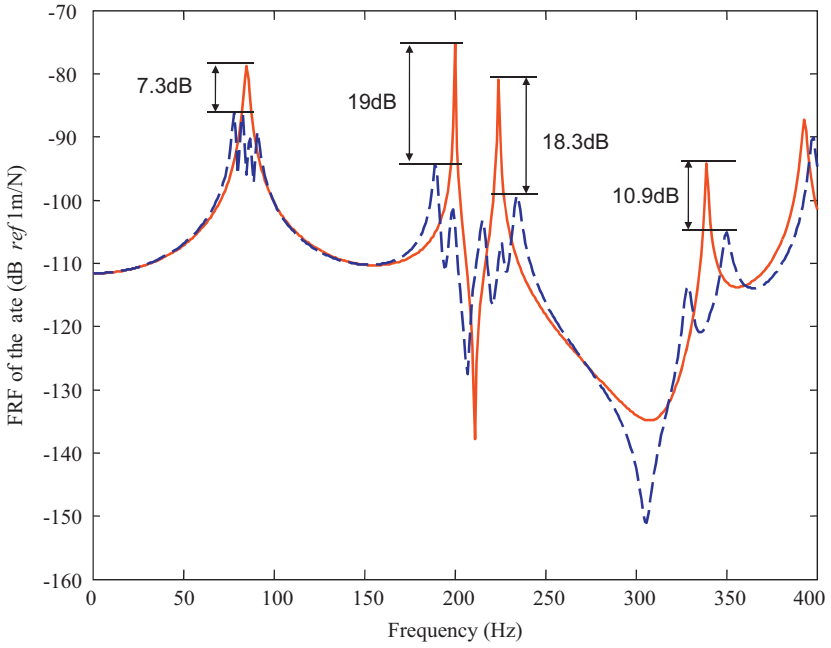

Fig. 17. FRF of the plate observed at (0.17 m, 0.20 m). ——, without DVAs; — —, with 12 optimized DVAs.

the determination of all resonance frequencies, the GA method is applied again to find the new optimal locations for all DVAs. In this study, four dominating modes are selected as the control target. For each mode, it is found that three DVAs can provide a desired band control performance. Notice that only DVA location is considered in the optimization. The FRF of the plate observed at (0.17 m, 0.20 m) is shown in Fig. 17 and the DVA parameters are listed in Table 2. It can be seen that an apparent reduction is achieved at each targeted mode, with reduction ranging from 7.3 to 19.0 dB.

Table 2
Optimized DVA locations.

Targeted mode	DVA resonance freq. (Hz)	Location (m)
	80	(0.2138, 0.2506)
(1, 1)	85	(0.2283, 0.2771)
	89	(0.2219, 0.2647)
	194	(0.2573, 0.3106)
(1, 2)	200	(0.1495, 0.2259)
	206	(0.2348, 0.2877)
	218	(0.2637, 0.18)
(2, 1)	224	(0.2106, 0.3053)
	230	(0.1351, 0.1253)
	333	(0.1994, 0.2506)
(2, 2)	339	(0.0949, 0.0953)
	345	(0.1929, 0.2153)

m_m=0.01, kg, ξ=0.01.

5. Conclusions

In this paper, a dynamic vibration absorber is used to suppress the vibration of a plate in a frequency band. The control mechanism is investigated with respect to different bandwidth, and the coupling is also examined in terms of the resonator location and frequency bandwidth. With the help of a mathematical model, it is found that the control mechanism of the DVA depends on the frequency bandwidth: for a narrow band control, the interaction between the DVA and the host structure by means of the reacting force from the absorber dominates the control performance; as the bandwidth gradually increases, there is a growing importance of energy dissipation; for a relatively wide band control, the energy dissipation of the DVA becomes a dominant factor.

Insertion of the DVA into the host structure activates more structural modes and revitalizes a more active modal coupling. This enhanced coupling depends not only on the bandwidth to be considered but also on the location of the DVA, which further influences the separation of the new coupled peaks.

For the control of well-separated modes, the optimal location of the DVA is found at the maximum vibration locations, in both narrow band and broadband control. For close-packed mode, however, the optimal location for installing DVA should be meticulously determined with the consideration of multi-modal coupling. Meanwhile, it is also possible to use the criteria provided in this work to suppress the adverse effect on the off-targeted mode without compromising the control performance at the targeted mode.

It should be stressed that the finding of the present work should not be limited to the case of a plate. In fact, based on modal expansion, the coupled equations of any structure can be decomposed into a set of discrete modal equations under a unified frame. Therefore, the mathematical equation, cast into the modal form, will be general enough to represent a general vibrating structure. In the present case, a simply-supported plate was chosen as a benchmark problem basically because of its simplicity. The conclusion drawn from it, however, remains general and applicable to any vibrating structures.

References

[1] J. Ormondroyd, J.P. Den Hartog, The theory of dynamic vibration absorber, *Journal of Applied Mechanics* 50 (1928) 9–22.
[2] D. Young, Theory of dynamic vibration absorbers for beams, *Proceedings of the First U.S. National Congress of Applied Mechanics*, New York, 1952, pp. 91–96.
[3] J.C. Snowdon, Vibration of cantilever beams to which dynamic absorbers are attached, *Journal of Acoustical Society of America* 39 (1966) 878–886.
[4] J.D. Van Dyke, J.W. Schendel, C.O. Gunderson, M.R. Bailard, Cabin noise reduction in the DC-9, *Commercial Aircraft Design and Operation Meeting*, Los Angeles, 1967, pp. 401–414.
[5] J.B. Hunt, *Dynamic Vibration Absorbers*, Mechanical Engineering Publications LTD, London, 1979.
[6] A.G. Thompson, Optimum tuning and damping of a dynamic vibration absorber applied to a force excited and damped primary system, *Journal of Sound and Vibration* 77 (1981) 403–415.
[7] P.L. Walsh, J.S. Lamancusa, A variable stiffness vibration absorber for the minimization of transient vibrations, *Journal of Sound and Vibration* 158 (1992) 195–211.
[8] M. Abdel-Rohman, Effectiveness of active TMD for buildings' control, *Transactions of the Canada Society of Mechanical Engineers* 8 (1984) 179–184.
[9] J.P. Den Hartog, *Mechanical Vibration*, McGraw-Hill, New York, 1956.
[10] J.C. Snowdon, *Vibration and Shock in Damped Mechanical Systems*, John Wiley & Sons, New York, 1968.
[11] R.G. Jacquot, W. Soedel, Vibrations of elastic surface systems carrying dynamic elements, *Journal of Acoustical Society of America* 47 (1970) 1354–1358.
[12] R.G. Jacquot, The forced vibration of singly modified damped elastic surface systems, *Journal of Sound and Vibration* 48 (1976) 195–201.
[13] J.W. Nicholson, L.A. Bergman, Vibration of damped plate-oscillator systems, *Journal of Engineering Mechanics* 112 (1986) 14–30.
[14] C.R. Fuller, J.P. Mailard, M. Mercadal, A.H. von Flotow, Control of aircraft interior noise using globally detuned vibration absorbers, *Journal of Sound and Vibration* 203 (1997) 745–761.
[15] D.A. Rade, V. Steffen, Optimisation of dynamic vibration absorbers over a frequency band, *Mechanical Systems and Signal Processing* 14 (2000) 679–690.
[16] R.G. Jacquot, Suppression of random vibration in plates using vibration absorbers, *Journal of Sound and Vibration* 248 (2001) 585–596.
[17] M.J. Brennan, J. Dayou, Global control of vibration using a tunable vibration neutralizer, *Journal of Sound and Vibration* 232 (2000) 585–600.
[18] R.G. Jacquot, Optimal damper location for randomly forced cantilever beams, *Journal of Sound and Vibration* 269 (2004) 623–632.

[19] C.Q. Howard, C.H. Hansen, A. Zander, Vibro-acoustic noise control treatments for payload bays of launch vehicles: discrete to fuzzy solutions, *Applied Acoustics* 66 (2005) 1235–1261.
[20] C. Yang, Dynamic Analysis of a Plate Incorporating DVAs and Tunable DVA Design, MSc Dissertation, The Hong Kong Polytechnic University, 2009.
[21] D.J. Ewins, *Modal Testing: Theory and Practice*, John Wiley & Sons, New York, 1984.
[22] R.W. Clough, J. Penzin, *Dynamics of Structures*, second ed, McGraw-Hill, New York, 1993.
[23] I.A. Karnovsky, O.I. Lebed, *Free Vibration of Beams and Frames*, McGraw-Hill, New York, 2004.
[24] G.H. Yu, L. Cheng, Location optimization of a long T-shaped acoustic resonator array in noise control of enclosures, *Journal of Sound and Vibration* 328 (2009) 42–56.